PHYSICAL REVIEW E **94**, 032701 (2016)

# Dynamics of electro-orientation of birefringent microsheets in isotropic and nematic liquid crystals

M. V. Rasna,[1] K. P. Zuhail,[1] U. V. Ramudu,[2] R. Chandrasekar,[2] and Surajit Dhara[1,*]
[1]*School of Physics, University of Hyderabad, Hyderabad 500046, India*
[2]*School of Chemistry, University of Hyderabad, Hyderabad 500046, India*
(Received 11 July 2016; published 29 September 2016)

We study the dynamics of electric field driven multiaxis electro-orientation of birefringent microsheets in both the isotropic and nematic phases of a liquid crystal. For a fixed direction of applied field in the isotropic phase, there are two critical fields above which the microsheets show two orientations. In the nematic phase, it shows three rotations in both planar and homeotropic cells. These orientations are observed at varying voltages and wide time scales and are explained based on the competing effect of the electric, elastic, and viscous torques. The control of the orientation of anisotropic microparticles (both optically and geometrically) by transducing external energy may be useful in electro-optics and photonics.

DOI: 10.1103/PhysRevE.94.032701

## I. INTRODUCTION

Studies on colloidal self-assembly have been one of the major driving themes in material science to obtain new functional and advanced materials. For example, making metamaterials requires control of the self-assembly of complex anisotropic colloidal particles such as toroids, coupled rods, and split ring resonators [1,2]. In this context, nematic liquid crystals (NLCs) have proven to be a potential medium for achieving predesigned, self-assembled structures. In NLCs a rich variety of structures are obtained by exploiting the long-range elastic interactions among dispersed colloids and the topological defects associated with them [3–7]. It has been suggested that tunability in such materials can be envisaged by external electric or magnetic fields [8–11]. In addition, there is a growing interest in studying the dynamics of the colloids in liquid crystals driven by external fields [12,13]. The collective response of these colloids may lead to new engineered materials and requires a proper understanding of their electrokinetics. Recently, in NLCs, several interesting electrokinetic responses of the colloids have been reported [11–15]. The majority of research on electric field driven dynamics in NLCs has reported on spherical colloids having isotropic optical and dielectric properties [8–11,14,15]. However, there are a few reports on the dynamics of nonspherical colloids in NLCs [11,14,16–18]. The dynamics of platelet-type colloids having optical and dielectric anisotropies is expected to be interesting. In this paper, we report the electric field driven multiaxis orientation of birefringent (single crystal) organic microsheets in both the isotropic and nematic phases of a liquid crystal. The electric field driven dynamics of single crystal microsheets promise potential applications in photonics and electro-optics.

## II. EXPERIMENT

Rectangular microsheets were prepared as per the reported procedure [19]. We used 5,10,15,20-tetra(*p*-tolyl)porphyrin as a building block to prepare nearly monodispersed microsheets [see Fig. 1(a)]. Microsheets are crystallized in tetrahydrofuran/water solvents. Typical lengths and widths are in the range of 9–10 $\mu$m and 4–5 $\mu$m, respectively. The average thickness of the microsheet is about 500 nm. A single crystal x-ray diffraction (XRD) study reveals the monoclinic structure of the crystals [19]. They are optically birefringent and the birefringence ($\Delta n$) of the microsheets is about 0.25 [5]. The orientation, interaction, and laser assisted self-assembly of the microsheets in a nematic liquid crystal have been reported by us recently [5].

The experimental cells with various spacings are fabricated by using indium-tin-oxide coated glass plates that are spin coated with polyimide AL-1254 and cured at 180 °C for 1 h. They were rubbed in the antiparallel direction for homogeneous alignment of the nematic director. For homeotropic alignment, we used JALS-204 and cured at 200 °C for 1 h. Sinusoidal voltage at 1 kHz is applied across the cell using a function generator (Tektronix-AFG 3102) and a voltage amplifier (TEGAM-2350), and the field direction is always perpendicular to the substrates. High-speed videomicroscopy is used for studying the rotational dynamics of isolated microsheets. We used pentyl cyano biphenyl (5CB), a positive dielectric anisotropy nematic liquid crystal ($\Delta\epsilon = 8.2$), and MLC-6608, a nematic mixture with negative dielectric anisotropy ($\Delta\epsilon = -4.2$) in the present study.

## III. RESULTS AND DISCUSSION

First, we present the field response of a microsheet in the isotropic phase of a 5CB liquid crystal. Figure 1(b) shows the schematic view of a microsheet with corresponding body axes along the length, breadth, and thickness. An isolated microsheet is selected, and the field-dependent response is recorded by the video camera (see S4:Video-1) [20]. Some representative images taken using polarizing optical microscope at various electric fields are shown in Figs. 1(c)–1(e). Usually, in the isotropic phase of the bulk sample, the microsheets are randomly oriented. However, in the cell when the cell thickness is not too large, most of the microsheets are parallel to the cell substrates [Fig. 1(c)]. When the applied field is in the range $E_1(=0.08\ \mathrm{V}/\mu\mathrm{m}) < E < E_2(=0.4\ \mathrm{V}/\mu\mathrm{m})$, the microsheets first rotate about the $x$ axis [Fig. 1(d)], and at higher fields, i.e., $E > E_2(=0.4\ \mathrm{V}/\mu\mathrm{m})$, they rotate about the $z$ axis [Fig. 1(e)]. These rotations are observed over a wide range of frequencies (100 Hz to 1 MHz) of the applied electric

*sdsp@uohyd.ernet.in

 

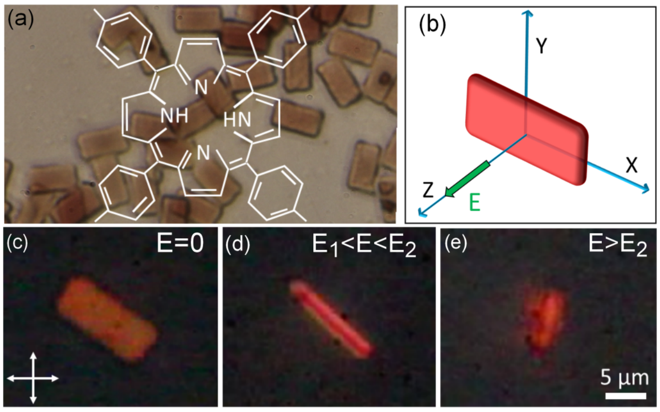


FIG. 1. (a) Optical microscopy image of the rectangular microsheets. The inset shows the chemical structure of the compound. (b) Schematic representation of the microsheet, with corresponding body axes $x$, $y$, and $z$ along the length, breadth, and thickness, respectively. (c)–(e) Electric-field-dependent multiaxis orientation of a microsheet in the isotropic phase of 5CB (see S4:Video-1 [20]). Sequence of polarizing optical microscopy images taken at different applied fields, (c) $E = 0$ V/$\mu$m, (d) $E_1 < E < E_2$, (e) $E > E_2$. The green arrow indicates the direction of the applied field (out of plane).

field. However. all the experiments in this study are done at a fixed frequency of 1 kHz that is much above the ionic charge relaxation frequency of 5CB liquid crystals. In the first rotation the electric-field-induced torque along the $x$ is greater than that of the $y$ axis (i.e., $\tau_x > \tau_y$). In the second rotation the torque along the $z$ axis is greater than that of the $y$ axis (i.e., $\tau_z > \tau_y$). Thus the orientation of microsheets in the isotropic phase can be controlled by the application of an external electric field.

To study the rotational dynamics, we applied a field, 0.75 V/$\mu$m($>E_2$), and observed two rotations around the $x$ and $y$ axes with time (see Fig. 2; S5:Video-2 [20]). The rotational dynamics of the dielectric particles under the action of electric field in isotropic liquids has been studied both experimentally and theoretically [1,21–26]. In those references, various types of microparticles are modeled as dielectric ellipsoids, and the dynamics is understood based on the competing effect of the electric-field-induced torque and hydrodynamic torque [21,24]. Here, we briefly mention the relevant torques acting on the particles. Total torque acting on a microsheet is given by $\tau = \tau_e + \tau_v$, where $\tau_e = 1/2\,\mathrm{Re}[\vec{P}\times\vec{E}]$ and $\vec{P} = \lambda\vec{E}$ gives the dipole moment, where $\lambda$ is the polarizability. The viscous torque can be written as $\tau_v = \zeta d\alpha/dt$, where $\zeta$ is the rotation constant, which depends on the medium viscosity, rotational hydrodynamic drag coefficient, and particle geometry [20]. The rotation angle about the $x$ axis, namely, $\alpha$ [the angle between the $y$ axis and field direction as defined in Fig. 2(d)] decreases from 90° to 0° [see S1(a) [20]]. The $x$ component of the electric torque is given by $\tau_e = \frac{1}{2}\Delta\lambda_1 E^2 \cos\alpha \sin\alpha$. This is balanced by the viscous torque, and the corresponding rotation rate can be describe by $\tan\alpha = \tan\alpha_0 \exp(-t/T_\alpha)$, where the time constant is given by $T_\alpha = \zeta/(E^2\Delta\lambda_1)$. The polarizability anisotropy is given by $\Delta\lambda_1 = (\lambda_y - \lambda_z)$, where $\lambda_y$ and $\lambda_z$ are the polarizabilities of the ellipsoid along the $y$ and $z$ directions [20]. Figure 2(g) shows a typical variation of $\tan\alpha$ with time.

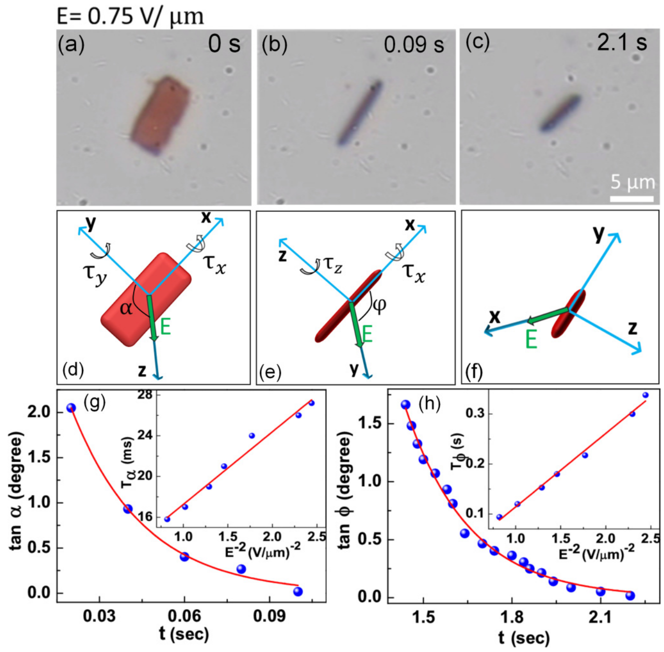


FIG. 2. (a)–(c) Time-dependent multiaxis rotation of a microsheet in the isotropic phase of 5CB for a fixed applied field, 0.75 V/$\mu$m($>E_2$) (see S5:Video-2 [20]). (d)–(f) Schematic representations of corresponding orientations. The green arrow indicates the direction of field. $\alpha$ defines the angle between the $y$ axis and the electric field. $\phi$ defines the angle between the $x$ axis and $E$. Variation of (g) $\tan\alpha$ and (h) $\tan\phi$ with time. Red curves show the best fit to the experimental data. Insets: Variation of $T_\alpha$ and $T_\phi$ with $1/E^2$. The red lines are the best fits.

This experiment was performed at various fields, and the time constant of the decay ($T_\alpha$) is found to be linearly proportional to $1/E^2$ [the inset of Fig. 2(g)], and the slope of the linear fit is given by $\zeta/\Delta\lambda_1 = 0.0071$ s(V/$\mu$m)$^{-2}$. After completing the rotation about the $x$ axis, the microsheet rotates about the $z$ axis and this rotation is slower than the rotation along the $x$ axis. In the second rotation, $\phi$ [the angle between the $x$ axis and field direction as defined in Fig. 2(e)] decreases from 90° to 0° [see S1(b) [20]], and the rate of rotation can again be described by $\tan\phi = \tan\phi_0 \exp(-t/T_\phi)$, where $T_\phi = \zeta/(E^2\Delta\lambda_2)$ and $\Delta\lambda_2 = \lambda_x - \lambda_y$ [20]. Figure 2(h) shows a typical variation of $\tan\phi$ with time. This experiment was also repeated at various fields and the time constant of the decay ($T_\phi$) is found to be proportional to $1/E^2$ [see the inset of Fig. 2(h)]. The slope of the linear fit is given by $\zeta/\Delta\lambda_2 = 0.1469$ s(V/$\mu$m)$^{-2}$. In the isotropic phase two independent rotations around two mutually orthogonal axes suggest that the microsheets are dielectrically anisotropic. In this context it may be recalled that from the x-ray diffraction studies it was found that the particles have a monoclinic crystal structure [19].

In the nematic phase, first we discuss the rotation of the microsheets in the planar cell below the Freedericksz threshold field (see S6:Video-3) [20]. The microsheet does not respond to the field below a critical value ($E_3$) and the plane of the microsheet is parallel to the substrate [Fig. 3(a)]. There is an intermediate and narrow field range, $E_3$(0.09 V/$\mu$m) $< E <$ $E_f$(=0.11 V/$\mu$m) ($E_f$ is the Freedericksz threshold field), in

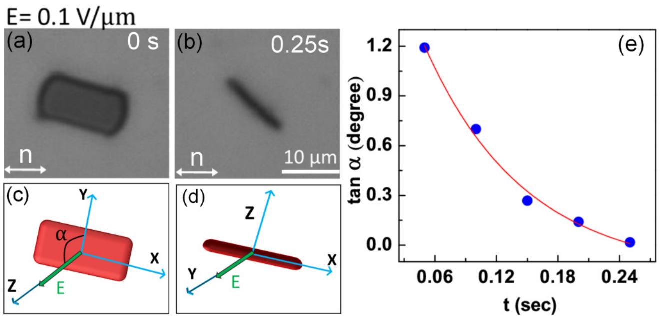


FIG. 3. Time-dependent rotation of a microsheet in nematic planar cell (5CB) below the Freedericksz threshold field. (a), (b) Sequence of images for the applied field $E = 0.1$ V/$\mu$m in 5CB at different times, where $E_3(=0.09$ V/$\mu$m$) < E < E_f(=0.11$ V/$\mu$m$)$. Schematic top view of the microsheet for (c) $E < E_3$ and (d) $E_3 < E < E_f$. $\alpha$ defines the angle between the $y$ axis and field direction. (e) Variation of $\tan\alpha$ as a function of time, and the red line shows the best fit (see S6:Video-3 [20]). **n** represents director (the average alignment direction of the LC molecules).

which the microsheet rotates about the $x$ axis, and the angle $\alpha$ [the angle between the $y$ axis and field direction as defined in Fig. 3(c)] decreases from 90° to 0° [Figs. 3(a) and 3(b); see also S2 [20]). This rotation is due to the electric-field-induced torque and is similar to that observed in the isotropic phase [Figs. 2(a) and 2(b)], but is somewhat slower compared to the isotropic phase. In particular, in the isotropic phase, the rotation was completed in less than 0.1 s [Fig. 2(g)], whereas in the nematic phase it took about 0.24 s [Fig. 3(e)]. This rotation is also due to the competing effects of viscous and electric torques, as discussed previously. Hence it is legitimate to use the same model and neglect the effect of small elastic torque experienced by the microsheets while rotating. Figure 3(e) shows the time variation of $\tan\alpha$ and the corresponding fit to $\tan\alpha = \tan\alpha_0 \exp(-t/T_\alpha)$. The time constant obtained, $T_\alpha =$ 100 ms, is much larger than that of the isotropic phase [see Fig. 2(g)]. This is expected as $T_\alpha$ is directly proportional to the average viscosity of the medium.

Now we discuss the rotation of the microsheets at a field which is greater that the Freedericksz threshold field ($E_f = 0.11$ V/$\mu$m) (see S8:Video-4 [20]). Figure 4 shows the rotation of the microsheet at an applied field, $E =$ 0.4 V/$\mu$m. Since $E > E_f$, the nematic director reorients along the field direction and consequently the long axis of the microsheet gets oriented, followed by an in-plane tilt [the third image in Fig. 4(a)]. These rotations are somewhat similar to those reported in square-type platelets with a hole in the middle (made of SU-8 photoresist) [11], except the final orientation of the microsheet is very different in the present case. Figure 4(e) shows the variation of $\phi(t)$ [the angle between the electric field and the body axis $x$ as defined in Fig. 4(b)] for two different field amplitudes. It can be fitted to a Boltzmann function $\phi(t) = (\phi_2 - \phi_1)/\{1 + \exp[(t - t_\circ)/T_\phi]\} + \phi_2$, where $(\phi_2 - \phi_1)$ is the total change of $\phi$, $t_\circ$ is the time at which $\phi(t) = (\phi_2 - \phi_1)/2$, and $T_\phi$ is the relaxation time. Figure 4(f) shows the relaxation time $T_\phi$ as a function of field. $T_\phi$ is expected to follow the following field dependence [11], $T_\phi = (\gamma d^2/\pi^2 K)[(E/E_f)^2 - 1]^{-1}$,

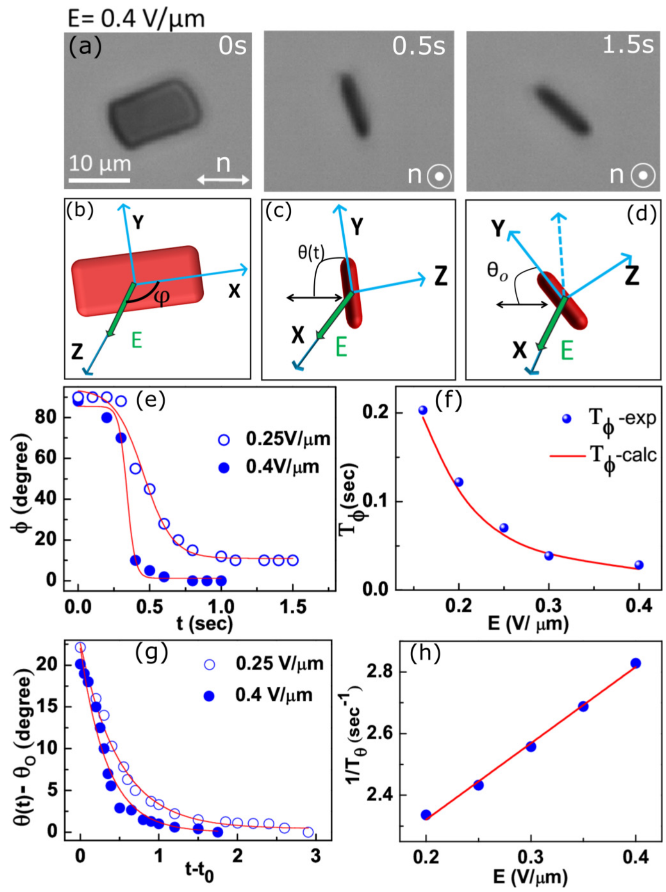


FIG. 4. Rotation of a microsheet in nematic planar cell (5CB) at a fixed field ($E = 0.4$ V/$\mu$m) (see S7:Video-4 [20]). (a) Sequence of images of the microsheet taken at different times. (b)–(d) Corresponding schematic top view. (e) Variation of $\phi(t)$ for two different field amplitudes, and the solid red line shows the best fits to the data with the Boltzmann function. (f) Relaxation time $T_\phi$, obtained from the fitting (circles) and calculated (red line), as a function of field. (g) Variation of in-plane rotation $\theta(t)$ for $E = 0.25$ V/$\mu$m and 0.4 V/$\mu$m. (h) Variation of $1/T_\theta$ with $E$. Red lines show the best fits to the experimental data. **n** indicates the director.

where $\gamma$ is the rotational viscosity, $d$ the cell thickness, and $K$ the average Frank elastic constant. Taking typical values $\gamma = 87$ mPa s, $K = 6.5$ pN, and $E_f = 0.11$ V/$\mu$m for 5CB, the calculated $T_\phi$ [solid red lines in Fig. 4(f)] agrees well with the experimental results. The in-plane rotation $\theta$ [see the third image in Fig. 4(a)] arises from the elastic interaction of the particle-induced distortions of the director and the field-dependent director deformations near the surface. For $E > E_f$ the splay bend deformation occurs over a height $h \approx (d/E)\sqrt{\frac{K}{\epsilon_o \Delta\epsilon}} \approx d(E_f/E\pi)$, where $K$ is the average elastic constant and $\Delta\epsilon$ is the dielectric anisotropy. The elastic free energy is given by [11] $F_{\rm el} \approx K(ac/\xi)(\theta - \theta_\infty)^2/2$, where $a$ and $c$ are the average length and thickness of the sheets. The elastic torque $\tau_{\rm el} = -\partial F_{\rm el}/\partial\theta \approx -K(\theta - \theta_\infty)ac/h$ is balanced by a viscous drag torque $\tau_v = \xi\eta d\theta/dt$, where $\xi$ is the rotational drag coefficient. The solutions of the equations of motion are exponential, $\theta(t) - \theta_0 = \theta_1 \exp(-t/T_\theta)$, where $\theta_0$ is the equilibrium angle and $T_\theta$ is the time constant,

$1/T_\theta = \pi Kac/(D^3\eta d)(E/E_f)$, where $d$ is the cell thickness and $D$ the diagonal length [11]. Figure 4(h) shows a linear variation of $1/T_\theta$ with $E$, and the corresponding slope is given by 1.9 $(\mathrm{sV}/\mu\mathrm{m})^{-1}$. Taking typical values $K = 6.5$ pN and $\eta = 25$ mPa s and other geometrical parameters of the microsheets, the calculated slope is $\simeq$1.3 $(\mathrm{sV}/\mu\mathrm{m})^{-1}$, which is very close to the experimental value despite the number of approximations made in the calculation.

The microsheet can be orientated vertically in a homeotropic cell. In this case a nematic liquid crystal with negative dielectric anisotropy is needed to study the electric field driven dynamics. For this purpose we have chosen a nematic mixture commercially known as MLC-6608. To study the dynamics we applied $E = 0.4$ V/$\mu$m, which is greater than the Freedericksz threshold field ($E_f = 0.16$ V/$\mu$m), and recorded the time-dependent rotations. The director reorients above the threshold field and consequently the microsheet rotates about the $y$ axis, followed by an in-plane rotation about the $z$ axis (see S8:Video-5) [20]. Figure 5(a) shows a series of images of rotation and Figs. 5(b)–5(d) show the corresponding schematic top views. After the in-plane rotation, it further rotates about the $x$ axis, making the $y$ axis parallel to the direction of the applied field. Figure 5(e) shows the plot of angle $\phi(t)$ (the angle between the direction of electric field and the $z$ axis of the microsheet) for two different field amplitudes. These can also be fitted with the Boltzmann function $\phi(t) = (\phi_2 - \phi_1)/\{1 + \exp[(t - t_\circ)/T_\phi]\} + \phi_2$, and the corresponding relaxation times $T_\phi$ at various fields are shown in Fig. 5(f). Taking typical values $\gamma = 0.186$ Pa s, $K = 17.4$ pN, and $E_f = 0.16$ V/$\mu$m, for MLC-6608, the calculated $T_\phi$ at room temperature agrees well with the experimental values. Figure 5(g) shows the time variation of the in-plane rotation angle $\theta$. It is observed that $\theta$ increases from zero and saturates to about 33° within 1 s. The rotation about the $x$ axis is due to the electric-field-induced torque, and the corresponding angle of rotation is defined as $\alpha$ [the angle between the $y$ axis and the field direction as defined in Fig. 5(c)]. The variation of $\alpha$ with time is given in the Supplemental Material [20]. Figure 5(h) shows the time variation of $\tan\alpha$ together with the best fit to $\tan\alpha = \tan\alpha_0 \exp(-t/T_\alpha)$. The time constant ($T_\alpha$) varies linearly with $1/E^2$ [see the inset for Fig. 5(h)]. The slope of the linear fit is given by 0.015 $\mathrm{s(V/\mu m)^2}$. The ratio of the slopes obtained from the linear fit of $T_\alpha$ vs $1/E^2$ in the isotropic phase of 5CB [see the inset of Fig. 2(g)] and the nematic phase of MLC-6608 is 0.46, and this is comparable to the ratio of the average viscosities ($\eta_{\mathrm{iso}}^{5\mathrm{CB}}/\eta_N^{\mathrm{MLC\text{-}6608}} = 0.5$) of the respective phases. A notable difference between the final orientation (above the Freedericksz threshold field) in the nematic phase of 5CB and MLC-6608 may be mentioned. In 5CB, the $x$ axis of the microsheet is oriented parallel to the field, whereas in MLC-6608 the $y$ axis is orientated along the field direction.

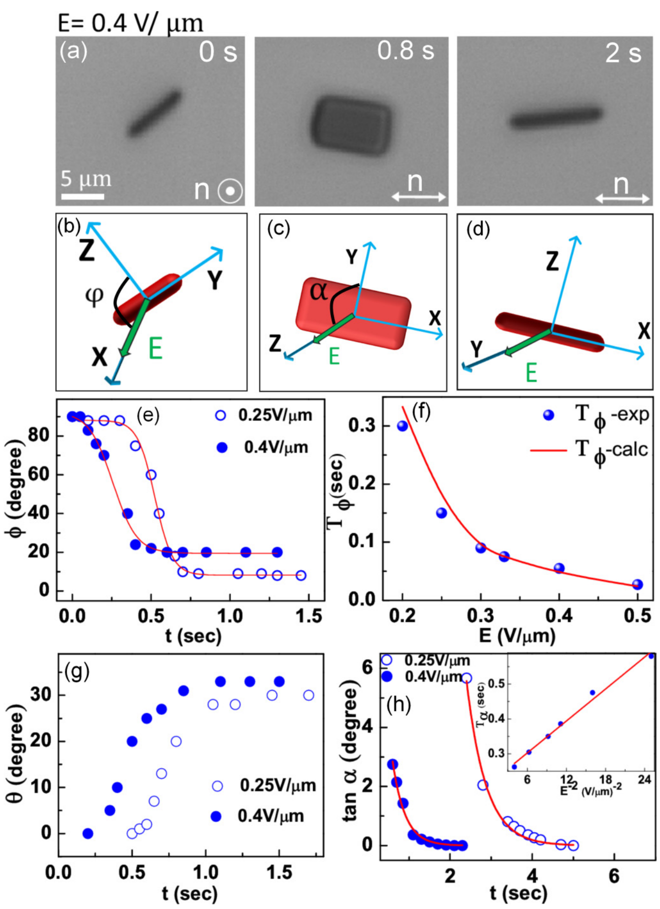


FIG. 5. Rotation of the microsheet in a homeotropic cell of MLC-6608 liquid crystal under the action of a fixed field, $E = 0.4$ V/$\mu$m ($> E_f$) (see S8:Video-5 [20]). (a) Sequence of images taken at different times and (b)–(d) corresponding schematic top views. (e)–(g) Time variation of rotation angles $\phi$ and $\theta$ for two different field amplitudes; the red curve in (e) shows the best fit to the Boltzmann function. (f) Variation of experimental relaxation time $T_\phi$ with field, together with the calculated values (red lines) for MLC-6608. (h) Variation of $\tan\alpha$ with time; red lines give the exponential fitting. Inset: Linear variation of $T_\alpha$ with $1/E^2$. **n** indicates the director.

## IV. CONCLUSION

In conclusion, we have shown that by applying a unidirectional electric field, birefringent microsheets can be rotated about multiple axes both in the isotropic and nematic phases of liquid crystals. Both positive and negative dielectric anisotropy liquid crystals are studied in the experiment. Two rotations in the isotropic phase are due to the electric-field-induced torques and suggest that the microsheets are dielectrically biaxial. In nematic planar and in homeotropic cells a total of six rotations are observed due to the interplay between electric, elastic, and hydrodynamic torques of the liquid crystal medium. The rate of rotation depends on the amplitude of the applied field and the average viscosity of the medium. A liquid crystal mediated rearrangement of optically anisotropic colloids may be potentially useful in applications in the field of photonics, for developing reconfigurable composites for metamaterials, and for understanding active matter. The analysis may also be helpful for the biophysical studies of anisotropic biological particles.

## ACKNOWLEDGMENTS

We gratefully acknowledge the support from the DST (DST/SJF/PSA-02/2014-2015), and DST-PURSE. M.V.R. acknowledge UGC-BSR for support through a fellowship grant.

[1] V. G. Veselago, Sov. Phys. Usp. **10**, 509 (1968).
[2] J. B. Pendry, Phys. Rev. Lett. **85**, 3966 (2000).
[3] I. Musevic, M. Skarabot, U. Tkalec, M. Ravnik, and S. Zumer, Science **313**, 954 (2006).
[4] U. Tkalec, M. Skarabot, and I. Musevic, Soft Matter **4**, 2402 (2008).
[5] M. V. Rasna, K. P. Zuhail, U. V. Ramudu, R. Chandrasekar, J. Dontabhaktuni, and S. Dhara, Soft Matter **11**, 7674 (2015).
[6] J. Dontabhaktuni, M. Ravnik, and S. Zumer, Proc. Natl. Acad. Sci. USA **111**, 2464 (2014).
[7] B. Senyuk, Q. Liu, E. Bililign, P. D. Nystrom, and I. I. Smalyukh, Phys. Rev. E **91**, 040501(R) (2015).
[8] K. Tagashira, K. Asakura, G. Nakazawa, and H. Yoshida, and M. Ozaki, AIP Adv. **2**, 042156 (2012).
[9] A. Nych, U. Ognysta, M. Skarabot, M. Ravnik, S. Zumer, and I. Musevic, Nat. Commun. **4**, 1489 (2013).
[10] M. Humar, M. Skarabot, M. Ravnik, S. Zumer, I. Poberaj, D. Babic, and I. Musevic, Eur. Phys. J. E **27**, 73 (2008).
[11] C. P. Lapointe, S. Hopkins, T. G. Mason, and I. I. Smalyukh, Phys. Rev. Lett. **105**, 178301 (2010).
[12] O. D. Lavrentovich, Curr. Opin. Colloid Interface Sci. **21**, 97 (2016).
[13] O. D. Lavrentovich, Soft Matter **10**, 1264 (2014).
[14] G. Liao, I. I. Smalyukh, J. R. Kelly, O. D. Lavrentovich, and A. Jakli, Phys. Rev. E **72**, 031704 (2005).
[15] A. Jakli, B. Senyuk, G. Liao, and O. D. Lavrentovich, Soft Matter **4**, 2471 (2008).
[16] Q. Liu, Ye Yuan, and I. I. Smalyukh, Nano Lett. **14**, 4071 (2014).
[17] Y. Zhang, Q. Liu, H. Mundoor, Y. Yuan, and I. I. Smalyukh, ACS Nano **9**, 3097 (2015).
[18] B. Senyuk, Q. Liu, S. He, R. D. Kamien, R. B. Kusner, T. C. Lubensky, and I. I. Smalyukh, Nature (London) **493**, 200 (2013).
[19] N. Chandrasekar, S. Basak, M. A. Mohiddon, and R. Chandrasekar, ACS Appl. Mater. Interfaces **6**, 1488 (2014).
[20] See Supplemental Material at http://link.aps.org/supplemental/10.1103/PhysRevE.94.032701 for multimedia videos and a few graphs.
[21] T. B. Jones, *Electromechanics of Particles* (Cambridge University Press, Cambridge, UK, 1995).
[22] J. A. Stratton, *Electromagnetic Theory* (McGraw-Hill, New York, 1941).
[23] I. Minoura and E. Muto, Biophys. J. **90**, 3739 (2006).
[24] P. Kang, X. Serey, Y. F. Chen, and D. Erickson, Nano Lett. **12**, 6400 (2012).
[25] R. C. Castberg, Z. J. Rozynek, E. G. Flekkøy, and K. J. Maloy, Front. Phys. (2016), doi:10.3389/fphy.2016.00001.
[26] D. Morganti and H. Morgan, Colloids Surf. A **376**, 67 (2011).